SACLANTCEN REPORT
serial no.: SR-194

SACLANT UNDERSEA
RESEARCH CENTRE

REPORT

Perturbation theory applied to sound scattering from a rough sea-floor

H.-H. Essen

September 1992

Page count for SR-194
(excluding covers)

Pages	Total
i–vi	6
1–21	21
	27

SACLANT Undersea Research Centre
Viale San Bartolomeo 400
19138 San Bartolomeo (SP), Italy

tel: 0187 540 111
fax: 0187 524 600
telex: 271148 SACENT I

NORTH ATLANTIC TREATY ORGANIZATION

SACLANTCEN SR-194

Perturbation theory applied to sound scattering from a rough sea-floor

H.-H. Essen

The content of this document pertains to work performed under Project 23 of the SACLANTCEN Programme of Work. The document has been approved for release by The Director, SACLANTCEN.

for John H. Foxwell
Director

intentionally blank page

SACLANTCEN SR-194

Perturbation theory applied to sound scattering from a rough sea-floor

H.-H. Essen

Executive Summary: Sound scattering from the sea-floor is of great importance for sonar performance This is true not only for the estimation of reverberation (i.e. limiting acoustic ranges), but also for detecting mines by acoustic means. While the first task mainly concerns low frequencies, the second requires high frequencies.

Scattering from the sea-floor is not yet well understood, mainly due to an insufficient knowledge of sea-floor parameters. Sea-floor roughness is considered to be the main source of scattering but inhomogeneities within the sea bed, such as buried stones in a sandy bottom, may also be of influence. Due to the shorter penetration, the latter effect can be assumed to be less important for higher frequencies.

This report shows that, contrary to statements in the literature, perturbation theory yields useful results when applied to sound scattering from a rough sea-floor. Indeed, important features of measured backscattering strengths can be explained by the theory. These are the absolute value of scattering strength, its independence of frequency over a wide range, and the observed dependence on grazing angle from nearly grazing to nearly perpendicular. It is shown that the necessary assumptions on the roughness spectrum of the sea-floor are reasonable.

Recommendations for future work are: (1) perturbation theory should be applied to interpret observed (mainly high-frequency) sea-floor scatter; (2) it seems worthwhile to use scattering coefficients as predicted by perturbation theory for numerical modelling and to compare this against other approaches such as Lambert's law.

intentionally blank page

SACLANTCEN SR-194

Perturbation theory applied to sound scattering from a rough sea-floor

H.-H. Essen

Abstract: Perturbation theory is applied to acoustic scattering from a rough sedimental sea-floor. Realistic boundary conditions are used, i.e. continuity of pressure and the normal component of particle velocity. The scattering strength as a function of grazing and azimuthal angle of incident and scattered energy is derived, depending on acoustic frequency, the two-dimensional roughness spectrum of the sea-floor and the ratios of sound velocity and density of the sediment to water. For the special case of backscattering, theoretical scattering coefficients are compared with measured data from the literature. Under reasonable assumptions on the sea-floor parameters, good agreement between theory and measurement can be achieved.

Keywords: grazing angle ○ azimuthal angle ○ backscattering ○ sound velocity ○ sediment density

Contents

1 Introduction

Scattering from the sea surface and sea-floor is of great importance in underwater sound propagation. While there exists a great deal of theoretical and experimental work on the sea surface, investigations on the sea-floor are relatively rare. This is mainly due to the limited knowledge of sea-floor characteristics. A recent review of mainly theoretical work is given by Ogilvy (1991).

In this report the first-order perturbation approach is used to explain some features as observed in bottom reverberation. This relatively simple theory is suitable for our purpose of demonstrating the influence of boundary conditions on scattering features. After perturbation theory was successfully used to explain radar backscatter from a rough sea surface (Wright, 1968), it was also applied to acoustic scattering by a number of authors. Thorsos (1990) compares different theoretical approaches to acoustic scattering from a rough sea surface of known statistics and finds reasonable results for the perturbation approach.

Two assumptions are fundamental to the present study. First it is assumed that perturbation theory yields reasonable results even if the requirement for roughness amplitudes to be small compared to acoustic wavelength is not strictly fulfilled. Two-scale models may extend the applicability of the theory to more general conditions. Secondly, it is assumed that the roughness of the sea bottom is the dominant determining characteristic for backscattering from the sea-floor, as stated by Urick (1983).

In Sect. 2 the theoretical scattering coefficients are derived. Section 3 compares theoretical results with measured data. Most existing measured data of sea-floor scattering are from backscatter. For this reason, the comparison of theoretical and measured scattering coefficients has been restricted to this special case. Observed backscattering strength depends on bottom type, acoustic frequency and grazing angle. The absolute value of the backscattering coefficient, as well as the above-mentioned factors, should be reflected by the theoretical results. Sea-floor parameters affecting the theoretical scattering coefficient, are the ratios of density and sound velocity of water and sediment and the two-dimensional roughness spectrum. The absolute value of the backscattering coefficient as well as its dependence on frequency are mainly determined by the two-dimensional wavenumber spectrum of bottom roughness.

Apart from some measurements showing a linear increase of backscatter with frequency, most measured data are frequency independent (Bunchuk and Zhitkovskii,

1980; Urick, 1983). To reproduce this feature by the theoretically derived scattering strength, a k^{-3} dependence of the wavenumber spectrum has to be assumed. The roughness spectrum used for fitting observed data is discussed in Appendix A. A simple statistical model has been used to produce synthetic representations of the bottom roughness. It appears that the assumptions made concerning the total variance and the dependence of the roughness spectrum on wavenumber are reasonable in the sense that they represent possible roughness fields. Also the assumptions of the perturbation parameter and the extension of the area of spatial averaging do not conflict with the considered roughness spectrum.

Theoretical backscattering coefficients show an increase with increasing density, which is in general agreement with observations showing greater reverberation over rocky bottoms than over mud bottoms (Urick, 1983). Realistic densities only slightly affect the dependence on grazing angle, while the (unrealistic) assumption of a rigid bottom of infinite density yields a quite different dependence.

Both the sound-velocity of the sea-floor and the roughness spectrum determine the grazing-angle dependence of backscattering. Within the approximate range of grazing angles 5–45°, data may be approximated by simple $\sin^n$ laws, with $n = 1$ suggested by Bunchuk and Zhitkovskii (1980) and $n = 2$ (Lambert's rule) by Urick (1983). For larger grazing angles the backscattering strength shows a strong rise with increasing angle, which is not represented by these empirical functions. Specular reflection from randomly distributed bottom facets has been used to explain this feature (Ellis and Crowe, 1991). The backscattering coefficient derived by perturbation theory describes the grazing-angle dependence well for both angle ranges. Moreover, it predicts a nonmonotonic behaviour of the backscattering strength with grazing angle exceeding the critical angle of total reflection. Evidence for this behaviour may be found in reverberation measurements, such as those made by Robison (1975) at 123 sites in different areas of the North Atlantic and those published by Ellis and Crowe (1991).

2

Perturbation theory

A cartesian coordinate system is used with the mean surface in the plane $z = 0$, and z pointing upwards. Incident acoustic energy arrives from above, in accordance with the geometry at the sea-floor. This geometry can also be applied to surface scattering, because it does not influence the results in term of scattering coefficients.

For simplicity we will consider the scattering of plane acoustic waves. The incident wave is described by

$$p_0 = A_0 \exp[i(\mathbf{k}_0 \cdot \mathbf{x} - \gamma_0 z - \omega t)] + \text{c.c.}, \tag{2.1}$$

with acoustic pressure p, wavenumber vector $\mathbf{k}_0 = [k_0 \cos\varphi_0, k_0 \sin\varphi_0]$, horizontal wavenumber $k_0 = (\omega/c_w)\cos\vartheta_0$, vertical wavenumber $\gamma_0 = (\omega/c_w)\sin\vartheta_0$, circular frequency ω, and sound velocity c_w.

Bold letters are used to represent two-dimensional horizontal vectors. Horizontal angles count anticlockwise from the x-axis (mathematical convention), and vertical angles from the surface, i.e. they are grazing angles. The complex conjugate solution (c.c.) is added in order to get real field variables.

The (infinite) interface is described by $z = \zeta(\mathbf{x})$ and may be represented by a two-dimensional Fourier integral

$$\zeta = \int Z(\mathbf{k}) \exp[i(\mathbf{k} \cdot \mathbf{x})]\, \mathrm{d}\mathbf{k}, \tag{2.2}$$

with $\mathbf{k} = [k\cos\varphi, k\sin\varphi]$, and $Z(-\mathbf{k}) = Z^*(\mathbf{k})$. The latter condition is introduced for obtaining real values of ζ and is appropriate for the frozen sea-floor. In the case of a moving sea surface, the wavenumber vector indicates the direction of phase velocity, and waves travelling in opposite directions have to be distinguished. Then the complex conjugate integral has to be added in (2.2). In other words, the Fourier components $Z(\mathbf{k})$, as defined by (2.2), contain the variance of waves travelling in opposite directions, which may not be distinguished in the case of the frozen sea-floor.

The sea-floor is assumed to be a zero-mean homogeneous random process:

$$\begin{aligned} \langle Z(\mathbf{k}) \rangle &= 0, \\ \langle Z(\mathbf{k}) Z^*(\mathbf{k}') \rangle &= F(\mathbf{k}) \delta(\mathbf{k} - \mathbf{k}'). \end{aligned} \tag{2.3}$$

with $\langle \zeta^2 \rangle = \int F(\mathbf{k})\, \mathrm{d}\mathbf{k}$. The angle brackets indicate ensemble means. The decorrelation of the Fourier amplitudes follows from the assumption of homogeneity. In this case the covariance function depends on the spatial lag between positions only and not on the position itself, and is the cosine transform of the variance spectrum $F(\mathbf{k})$. It should be mentioned that the integral is taken over the whole wavenumber circle with identical contributions from wavenumbers of opposite direction.

The boundary conditions at the sea-floor require continuity of pressure and normal component of particle velocity,

$$\begin{aligned} p_\mathrm{w} - p_\mathrm{b} &= 0, \\ w_\mathrm{w} - w_\mathrm{b} - (\mathbf{u}_\mathrm{w} - \mathbf{u}_\mathrm{b}) \cdot \nabla\zeta &= 0, \quad \text{at } z = \zeta, \end{aligned} \tag{2.4}$$

with vertical component of particle velocity w, horizontal vector of particle velocity $\mathbf{u} = [u, v]$, and $\nabla = [\partial/\partial x, \partial/\partial y]$. The indices w and b refer to the upper fluid and lower sediment half-space, respectively.

In both media (m = w or b) the same equations of motion are valid but with different values of sound velocity c and density ρ:

$$\begin{aligned} \frac{\partial^2 p_\mathrm{m}}{\partial t^2} - c_\mathrm{m}^2 \left(\frac{\partial^2 p_\mathrm{m}}{\partial x^2} + \frac{\partial^2 p_\mathrm{m}}{\partial y^2} + \frac{\partial^2 p_\mathrm{m}}{\partial z^2} \right) &= 0, \\ \rho_\mathrm{m} \frac{\partial \mathbf{u}_\mathrm{m}}{\partial t} &= \nabla p_\mathrm{m}, \\ \rho_\mathrm{m} \frac{\partial w_\mathrm{m}}{\partial t} &= \frac{\partial p_\mathrm{m}}{\partial z} \end{aligned} \tag{2.5}$$

Approximate solutions of (2.4) and (2.5) may be obtained by means of perturbation theory, in which case the field variables can be expanded into convergent perturbation series:

$$\begin{aligned} p_\mathrm{m} &= p_\mathrm{m}^{(0)} + p_\mathrm{m}^{(1)} + \ldots, \\ \mathbf{u}_\mathrm{m} &= \mathbf{u}_\mathrm{m}^{(0)} + \mathbf{u}_\mathrm{m}^{(1)} + \ldots, \\ w_\mathrm{m} &= w_\mathrm{m}^{(0)} + w_\mathrm{m}^{(1)} + \ldots. \end{aligned} \tag{2.6}$$

Performing a Taylor expansion around the undisturbed interface and inserting the perturbation series (2.6), the zero- and first-order boundary conditions become

$$\begin{aligned} p_\mathrm{w}^{(0)} - p_\mathrm{b}^{(0)} &= 0, \\ w_\mathrm{w}^{(0)} - w_\mathrm{b}^{(0)} &= 0, \quad \text{at } z = 0, \end{aligned} \tag{2.7}$$

and

$$p_{\mathrm{w}}^{(1)} - p_{\mathrm{b}}^{(1)} = -\frac{\partial(p_{\mathrm{w}}^{(0)} - p_{\mathrm{b}}^{(0)})}{\partial z}\zeta,$$

$$w_{\mathrm{w}}^{(1)} - w_{\mathrm{b}}^{(1)} = (\mathbf{u}_{\mathrm{w}}^{(0)} - \mathbf{u}_{\mathrm{b}}^{(0)}) \cdot \nabla\zeta - \frac{\partial(w_{\mathrm{w}}^{(0)} - w_{\mathrm{b}}^{(0)})}{\partial z}\zeta, \quad \text{at } z = 0. \tag{2.8}$$

The zero-order solution yields the specular reflected wave in the fluid medium and a refracted wave in the sediment bottom:

$$p_{\mathrm{w}}^{(0)} = A_0 \exp[i(\mathbf{k}_0 \cdot \mathbf{x} - \gamma_0 z - \omega t)] + A_{\mathrm{r}} \exp[i(\mathbf{k}_0 \cdot \mathbf{x} + \gamma_0 z - \omega t)] + \text{c.c.},$$
$$p_{\mathrm{b}}^{(0)} = A_{\mathrm{t}} \exp[i(\mathbf{k}_0 \mathbf{x} - \kappa_0 z - \omega t)] + \text{c.c.}, \tag{2.9}$$

with $A_{\mathrm{r}} = (\alpha\gamma_0 - \kappa_0)A_0/(\alpha\gamma_0 + \kappa_0)$, $A_{\mathrm{t}} = 2\alpha\gamma_0 A_0/(\alpha\gamma_0 + \kappa_0)$, $\kappa_0 = \sqrt{(\omega/c_{\mathrm{b}})^2 - k_0^2}$, and $\alpha = \rho_{\mathrm{b}}/\rho_{\mathrm{w}}$. For small grazing angles, κ_0 becomes imaginary and total reflection occurs.

By inserting the zero-order solutions (2.9) into the first-order boundary conditions (2.8) and making use of the linear equations of motion within the media (2.5), one obtains

$$p_{\mathrm{w}}^{(1)} = \sum_{\sigma=\pm 1} \int B_{\mathrm{r}} \exp[i\sigma(\mathbf{k}_{\mathrm{s}} \cdot \mathbf{x} + \gamma_{\mathrm{s}} z - \omega t)] Z(\mathbf{k})\, \mathrm{d}\mathbf{k},$$
$$p_{\mathrm{b}}^{(1)} = \sum_{\sigma=\pm 1} \int B_{\mathrm{t}} \exp[i\sigma(\mathbf{k}_{\mathrm{s}} \cdot \mathbf{x} - \kappa_{\mathrm{s}} z - \omega t)] Z(\mathbf{k})\, \mathrm{d}\mathbf{k}, \tag{2.10}$$

with $\mathbf{k}_{\mathrm{s}} = \mathbf{k}_0 + \sigma\mathbf{k}$, $\gamma_{\mathrm{s}} = \sqrt{(\omega/c_{\mathrm{w}})^2 - k_{\mathrm{s}}^2}$, and $\kappa_{\mathrm{s}} = \sqrt{(\omega/c_{\mathrm{b}})^2 - k_{\mathrm{s}}^2}$.

Due to the quadratic coupling, two contributions occur, referring to the sum ($\sigma = +1$) and difference ($\sigma = -1$) of the interacting wavenumbers. The wavenumbers as well as the amplitudes of the scattered field depend on σ.

We are only interested in the acoustic field of the upper fluid half-space, i.e. the amplitude B_{r}:

$$B_{\mathrm{r}} = 2i\gamma_0 A_0/[(\alpha\gamma_0 + \kappa_0)(\alpha\gamma_{\mathrm{s}} + \kappa_{\mathrm{s}})]$$
$$\times [(\alpha - 1)[\alpha(\mathbf{k}_0 \cdot \mathbf{k}_{\mathrm{s}} - k_0^2) - \kappa_0\kappa_{\mathrm{s}}] - \alpha(\alpha\gamma_0^2 - \kappa_0^2)]. \tag{2.11}$$

When $\alpha = 0$ the acoustic field vanishes in the lower half-space and the solution refers to the free sea surface.

The perturbation expansion requires the first-order solution to be small in amplitude as compared to the incident wave. This obviously is the case if the perturbation parameter (or Rayleigh parameter), i.e. the product of vertical wavenumber $\gamma_0 = (\omega/c)\sin(\vartheta_0)$ and roughness amplitude $Z(\mathbf{k})$, is small compared to unity. At small grazing angles this may be true even for relatively large roughness amplitudes.

In order to compute scattered intensities, ensemble averaging (2.3) over the random interface (2.2) is performed. For real data, no ensemble is available and spatial averages have to be taken. It has to be assumed that the area considered is large compared to the correlation length of the random surface.

Taking the square of the scattered field within the fluid half-space in (2.10) and making use of the statistical properties of the scattering interface (2.3), the mean scattered acoustic intensity becomes

$$I_s = \langle p_w^{(2)} p_w^{(2)} \rangle = \sum_{\sigma=\pm 1} \int \mid B_r \mid^2 F(\mathbf{k})\, \mathrm{d}\mathbf{k}. \tag{2.12}$$

This equation may be simplified, as opposite signs of σ refer to opposite signs of the scattering wavenumber vector $\mathbf{k}$, which both yield the same contribution to the integral (2.12). Making use of (2.2) and (2.3) and replacing the scattering wavenumber of the interface by the difference between the incident and scattered acoustic wavenumber (2.10), one obtains

$$F(-\mathbf{k}) = F(\mathbf{k}) = F(\mathbf{k}_s - \mathbf{k}_0). \tag{2.13}$$

It should be mentioned that this simplification is not possible for a moving surface where contributions from opposite scattering wavenumber vectors may be different. Making use of (2.13), one obtains

$$I_s = 2 \int \mid B_r \mid^2 F(\mathbf{k}_s - \mathbf{k}_0)\, \mathrm{d}\mathbf{k}_s, \tag{2.14}$$

with $\mathbf{k}_s = \mathbf{k}_0 + \mathbf{k}$.

Changing the integration in (2.14) to φ_s and ϑ_s, the integral reads

$$I_s = 2(\omega/cw)^2 \iint \mid \mathrm{B_r} \mid^2 \mathrm{F}(\mathbf{k}_s - \mathbf{k}_0) \sin \#_s \cos \#_s \, \mathrm{d}'_s \, \mathrm{d}\#_s, \tag{2.15}$$

with $\mathbf{k}_s = (\omega/cw) \cos \#_s [\cos '_s, \sin '_s]$.

Now, the scattering coefficient S is defined (cf. Brekhovskikh and Lysanov, 1991) by

$$I_s = A_0^2 \int (S/r^2)\, \mathrm{d}\mathbf{a}, \tag{2.16}$$

where r is the distance from the scattering area to the reference point and the integration is carried out over the infinite bottom or surface. The dB value of the scattering coefficient is called the scattering strength. For geometrical reasons, the integral may be changed to

$$I_s = A_0^2 \iint S \cot \vartheta_s \, \mathrm{d}\varphi_s \, \mathrm{d}\vartheta_s. \tag{2.17}$$

Comparing (2.15) and (2.17), the scattering coefficient then becomes

$$S(\omega, \varphi_0, \vartheta_0, \varphi_s, \vartheta_s) = 2\left(\frac{\omega}{c_w}\right)^2 \mid \frac{B_r}{A_0} \mid^2 F(\mathbf{k}_s - \mathbf{k}_0)\sin^2(\vartheta_s). \tag{2.18}$$

This formula allows some conclusions with respect to scattering close to the specular direction. In this case the scattering wavenumbers become small, which means that scattering is due to the long waves of the roughness field. In general, these contain more variance than shorter waves and scattering in the near-specular direction becomes stronger.

Backscattering is of special interest. In this case, the condition

$$\mathbf{k}_s = -\mathbf{k}_0 \tag{2.19}$$

holds and the backscattering coefficient becomes

$$S_b(\omega, \varphi_0, \vartheta_0) = T_b F(2\mathbf{k}_0) \tag{2.20}$$

with $T_b = 4\gamma_0^4 \mid \alpha^2(2k_0^2 + \gamma_0^2) - 2\alpha k_0^2 - \kappa_0^2 \mid^2 / \mid \alpha\gamma_0 + \kappa_0 \mid^4$.

A vanishing subsurface density refers to a free surface, for which the transfer function T_b becomes

$$T_b(\omega, \varphi_0, \vartheta_0) = 4\gamma_0^4. \tag{2.21}$$

The variance spectrum, as defined by (2.3), refers to a frozen surface and represents the contributions from positive and negative wavenumbers in the case of a moving sea surface.

The backscattering coefficient of an absolutely rigid sea-floor is obtained in the limit of infinite density, which yields the tranfer function

$$T_b(\omega, \varphi_0, \vartheta_0) = 4(2k_0^2 + \gamma_0^2)^2. \tag{2.22}$$

It is worthwhile to notice that in this case, backscatter does not vanish for zero grazing angle.

3
Numerical results

An empirical scattering coefficient has been introduced by Mackenzie (1961) based on Lambert's rule:

$$S = S_0 \sin\vartheta_0 \sin\vartheta_s \tag{3.1}$$

with S_0 = constant. This relation is well known from optics and states the fact that for many materials an illuminated area looks almost equally bright when viewed from different angles. Lambert's rule contains no dependence on the roughness spectrum and predicts frequency-independent scattering coefficients. The respective backscattering coefficient becomes

$$S_b = S_0 \sin^2\vartheta_0. \tag{3.2}$$

In a review paper, Bunchuk and Zhitkovskii (1980) found that most backscattering measurements show a dependence on $\sin\vartheta_0$ for grazing angles below 50°. Urick (1983), as well as Ellis and Crowe (1991), prefers Lambert's rule. The scattering coefficient derived by means of perturbation theory shows a more complicated dependence, influenced by sea-floor parameters.

The representation of backscattering coefficients in dB (scattering strength) performs a decomposition into additive contributions from the transfer function and the spectral component of roughness (cf. (2.20)):

$$10\log(S_b) = 10\log(T_b) + 10\log(F(2\mathbf{k}_0)). \tag{3.3}$$

Considering the results of perturbation theory applied to a free surface, the first term in (3.3) yields a grazing-angle dependence of $\sin^4$ (cf. (2.21)), which is superimposed by a contribution from the roughness spectrum. The roughness spectrum is a function of the horizontal wavenumber, and thus of the acoustic frequency and the cosine of the grazing angle. Only in the unrealistic case of a constant spectrum (i.e. a white spectrum in both components of horizontal wavenumber) does the $\sin^4$ dependence of the transfer function also hold for the backscattering coefficient. However, the roughness spectrum is insensitive to variations in small grazing angles. Thus, for small grazing angles a $\sin^4$ dependence of the backscattering coefficient can be assumed.

Figure 1 compares different $\sin^n\vartheta_0$ functions with $n = 1$, $n = 2$, and $n = 4$, where the first two represent empirical approaches, and the latter arises from perturbation theory applied to scattering from a free surface at small grazing angles. Scattering

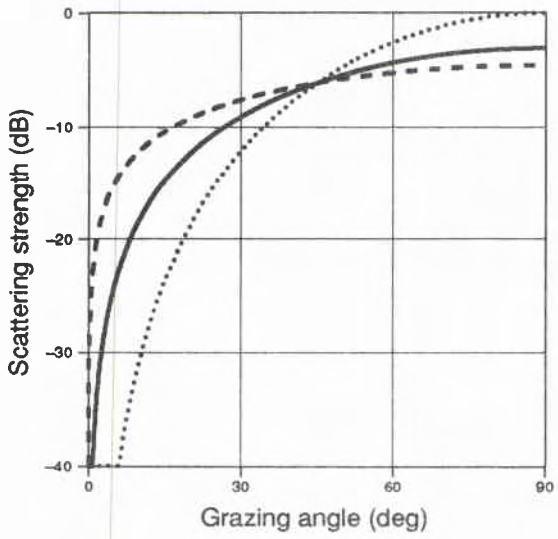

Figure 1 *Empirical backscattering strengths. Dashed curve:* $\sin\vartheta_0$. *Solid curve:* $\sin^2\vartheta_0$ *(Lambert's rule). Dotted curve:* $\sin^4\vartheta_0$.

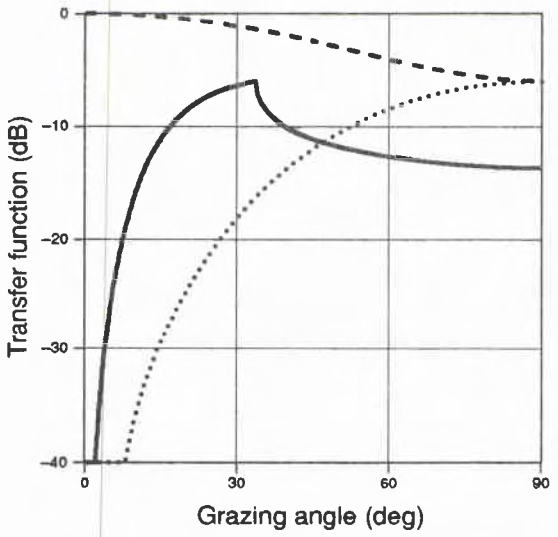

Figure 2 *Theoretical backscatter transfer functions for different surfaces. Dashed curve: rigid bottom* ($\rho_b = \infty$). *Solid curve: sedimental sea floor* ($c_b/c_w = 1.2$, $\rho_b/\rho_w = 2.0$). *Dotted curve: free surface* ($\rho_b = 0$).

strengths in Fig. 1 are arbitrarily normalized with the constraint of intersecting at grazing angle of 45°.

In order to show the influence of the boundary conditions involved, Fig. 2 displays the dependence of the transfer function on grazing angle for a free surface (2.21), a sediment bottom with realistic sound velocity and density (2.20), and an absolutely rigid bottom (2.22). The normalisation is arbitrary but the same for all three curves. Except for an additive constant, the dotted curve (scattering from a free surface) is the same as in Fig. 1. The three cases show distinctly different behaviours for all grazing angles. An important feature of the tranfer function of the sediment bottom is the nonmonotonic behaviour around the angle of total reflection (the critical angle). The transfer functions do not represent the backscattering coefficient, as the wavenumber spectrum also contributes angle dependence. However, for small graz-

ing angles this dependence is of less importance. For small grazing angles (i.e. below 30°), the comparison with Fig. 1 shows that the theoretical scattering coefficient for a sediment sea-floor may not be represented by a simple $\sin^n$ law.

The transfer function T_b (cf. (2.20)) is proportional to ω^4, indicating a strong frequency dependence, which on the other hand could not be observed in measured data. Thus, a sea-floor wavenumber spectrum is sought which compensates for the frequency dependence of the transfer function. As nothing else is known, it is reasonable to assume that the wavenumber spectrum is isotropic:

$$F(\mathbf{k}) = G(k)/(2\pi k). \tag{3.4}$$

$G(k)$ is the one-dimensional wavenumber spectrum which, by inserting (3.4) in (2.3), yields

$$\langle \zeta^2 \rangle = \int G(k)\,\mathrm{d}k. \tag{3.5}$$

Inserting (3.4) into (2.20), the backscattering coefficient becomes

$$S_b(\omega, \varphi_0, \vartheta_0) = T_b G(2k_0)/(4\pi k_0). \tag{3.6}$$

Through k_0 both the dependence on grazing angle and frequency are affected, decreasing the latter to ω^{-3}.

In general, roughness spectra decrease with increasing wavenumber. A reasonable assumption is a k^{-2} decay, which means that amplitudes are proportional to wavelength. Such spectrum leads to a linear increase of backscattering with frequency. Some of the measurements summarised by Urick (1983) show this rise in scattering strength with frequency, but most of the data show frequency-independent backscatter, in accordance with data presented by Bunchuk and Zhitkovskii (1980). For this reason, we introduce a wavenumber spectrum decaying by k^{-3}:

$$G(k) = G_0 k^{-3}. \tag{3.7}$$

It should be mentioned that by this assumption the factor G_0 is dimensionless. The backscattering coefficient becomes

$$S_b = T_b G_0/(32\pi k^4), \tag{3.8}$$

Insertion of the transfer function T_b of a free surface (2.21) yields

$$S_b = G_0 \tan^4 \vartheta_0/(8\pi). \tag{3.9}$$

The frequency independence of backscattering, as reported by Urick (1983) and Bunchuk and Zhitkovskii (1980), extends from about 2 kHz to 100 kHz, the backscattering strength for sediment sea-floor at a grazing angle of 30° varies around −30 dB. Fitting the theoretical backscattering coefficient to these data, we find

$$G_0 = 0.01. \tag{3.10}$$

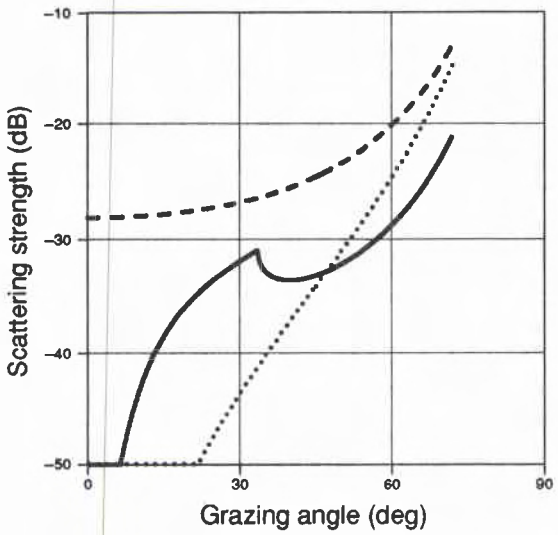

Figure 3a *Theoretical backscattering strengths for different surfaces,* $G(k) = 0.01k^{-3}$. *Dashed curve: rigid bottom* ($\rho_b = \infty$). *Solid curve: sedimental sea floor* ($c_b/c_w = 1.2$, $\rho_b/\rho_w = 2.0$). *Dotted curve: free surface* ($\rho_b = 0$).

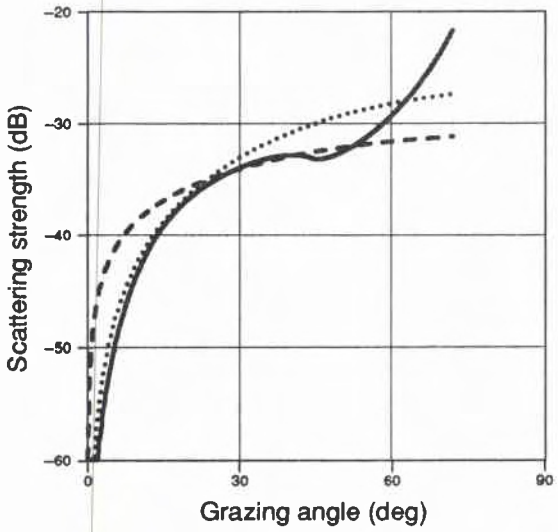

Figure 3b *Comparison of empirical and theoretical backscattering strengths. Dashed curve:* $\sin(\vartheta_0)$. *Dotted curve:* $\sin^2(\vartheta_0)$ *(Lambert's rule). Solid curve: theoretical backscattering strength with* $G(k) = 0.01k^{-3}$, *average over* $1.0c_w < c_b < 1.3c_w$, $1.6\rho_w < \rho_b < 2.1\rho_w$.

Representations of the roughness spectrum, defined by (3.7) and (3.10) are derived in Appendix A. It appears that the asssumptions made can be fulfilled by realistic roughness fields.

The backscattering strengths, presented in Fig. 3a, again show the strong dependence of backscatter on the type of interface. For small grazing angles, the angle dependence agrees well with that of the transfer function in Fig. 2. For larger grazing angles there is an increase of backscatter, which is also observed in measurements but cannot be represented by the empirical scattering coefficients of Fig. 1.

Figure 3b shows an averaged backscattering strength as function of grazing angle compared with the empirical $\sin^1$ and $\sin^2$ functions of Fig. 1. Averaging is performed over bottom-sound velocities in the range 1.0–$1.3c_w$ and respective densities

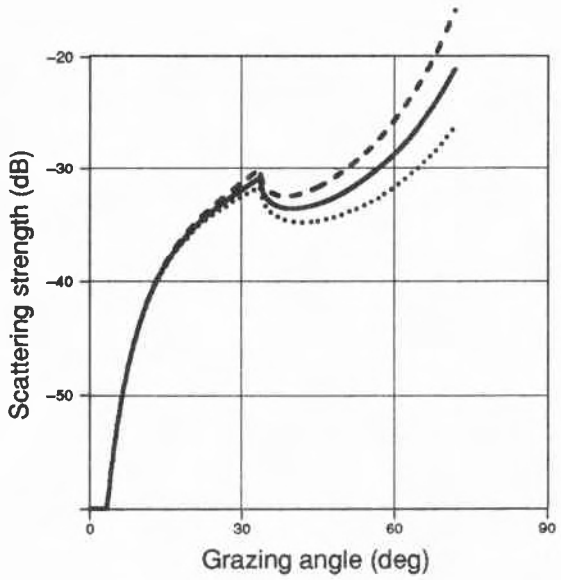

Figure 4a *Theoretical backscattering strengths for different k-dependences of roughness spectrum,* $c_b/c_w = 1.2$, $\rho_b/\rho_w = 2.0$. *Dotted curve:* $G(k) = 0.01(\omega_0/c_w)^{-1}k^{-2}$. *Solid curve:* $G(k) = 0.01k^{-3}$. *Dashed curve:* $G(k) = 0.01(\omega_0/c_w)k^{-4}$.

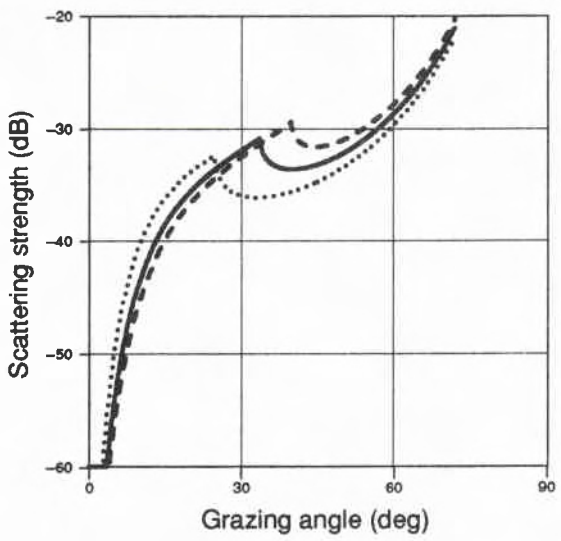

Figure 4b *Theoretical backscattering strengths for different seafloor sound velocities,* $\rho_b/\rho_w = 2.0$, $G(k) = 0.01k^{-3}$. *Dotted curve:* $c_b/c_w = 1.1$. *Solid curve:* $c_b/c_w = 1.2$. *Dashed curve:* $c_b/c_w = 1.3$.

in the range $1.6–2.1\rho_w$. This averaging is in accordance with the data of Bunchuk and Zhitkovskii (1980) and Urick (1983), representing mean values from different experimental sites. Bunchuk and Zhitkovskii (1980) state a $\sin^1$ dependence of the backscattering coefficient for grazing angles in the range 10–50°, while Urick (1983) suggests a $\sin^2$ dependence (Lambert's rule). Figure 3b shows a good agreement of the theoretical curve with Lamberts's rule at grazing angles below 25° while for higher grazing angles a $\sin^1$ dependence better fits to the flattening of the theoretical curve.

Theoretical backscattering coefficients depend on different parameters, such as the k-dependence of the roughness spectrum, the ratios of sediment to water sound

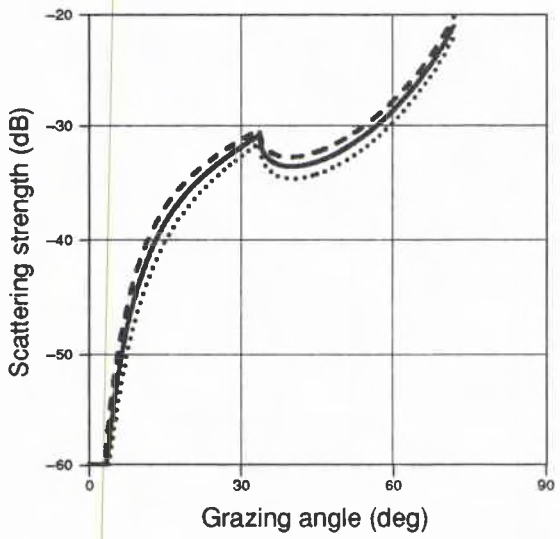

Figure 4c *Theoretical backscattering strengths for different sea-floor densities,* $c_b/c_w = 1.2$, $G(k) = 0.01k^{-3}$. *Dotted curve:* $\rho_b/\rho_w = 1.8$. *Solid curve:* $\rho_b/\rho_w = 2.0$. *Dashed curve:* $\rho_b/\rho_w = 2.2$.

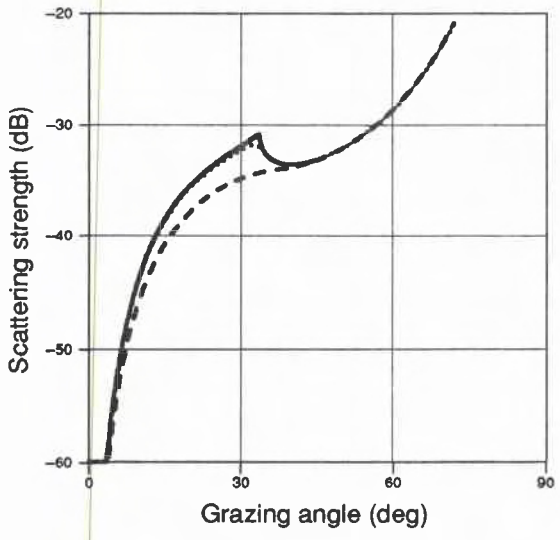

Figure 4d *Theoretical backscattering strengths for different bottom losses,* $c_b/c_w = 1.2$, $\rho_b/\rho_w = 2.0$, $G(k) = 0.01k^{-3}$. *Solid curve:* $c_{bI} = 0$. *Dotted curve:* $c_{bI}/c_w = 0.01$. *Dashed curve:* $c_{bI}/c_w = 0.1$.

velocity and density and also on the acoustic attenuation of the sea-floor (bottom loss). These parameters are investigated in Figs. 4a–d. Modifications are related to standard conditions, wavenumber spectrum as defined by (3.7) and (3.10), the ratios of sound velocities $c_b/c_w = 1.2$ and densities $\rho_b/\rho_w = 2.0$ in sediment and water, and no bottom loss. These are represented by a solid line throughout.

Figure 4a shows the dependence of the backscattering strength on the decay of the roughness spectrum. This is mainly seen at larger grazing angles, while smaller grazing angles are not affected. The steeper increase refers to a k^{-4} decay of the spectrum, implying a frequency dependence of the backscattering coefficient by ω^{-1}. Accordingly, the less steep curve refers to a k^{-2} decay and a linear increase of the backscattering coefficient with frequency.

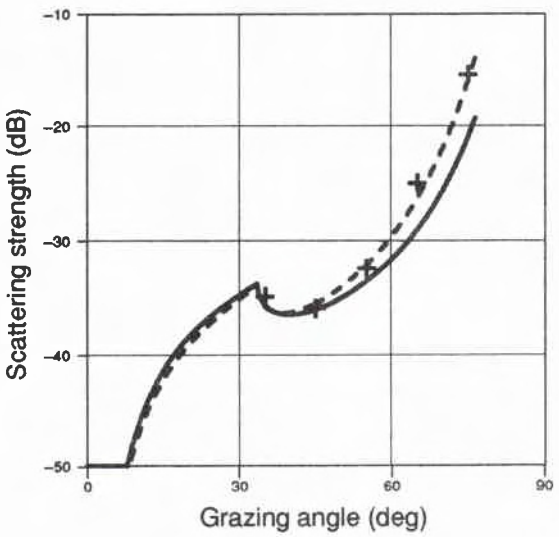

Figure 5a *Measured data fitted by theoretical backscattering strengths,* $c_b/c_w = 1.2$, $\rho_b/\rho_w = 2.0$. *Solid curve:* $G(k) = 0.005k^{-3}$. *Dashed curve:* $G(k) = 0.004(\omega_0/c_w)k^{-4}$. *Crosses: data from Ellis and Crowe (1991) of explosive measurements in a deep-water area.*

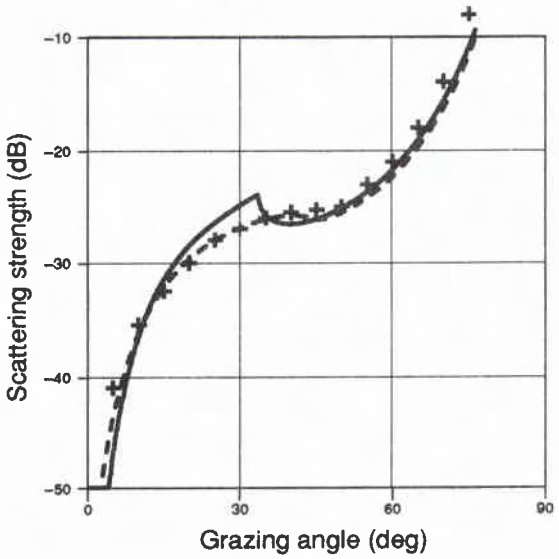

Figure 5b *Measured data fitted by theoretical backscattering strengths. Solid curve:* $c_b/c_w = 1.2$, $\rho_b/\rho_w = 2.0$, $G(k) = 0.05k^{-3}$. *Dashed curve: average over* $1.0c_w < c_b < 1.3c_w$, $1.6\rho_w < \rho_b < 2.1\rho_w$, $G(k) = 0.05k^{-3}$. *Crosses: data from Bunchuk and Zhitkovskii (1980) of mean values for a sandy sea floor and acoustic frequency range 10 kHz–100 kHz.*

Figure 4b displays backscattering strengths for different sound velocities of the sea-floor. Clearly, this parameter is very important, both for the absolute value as well as the dependence on grazing angle. In particular, the critical angle is determined by the sound-velocity ratio and with it the nonmonotonic interval of the backscattering strength as a function of grazing angle.

The dependence of the theoretical backscattering strength on the density of the sea-floor is shown in Fig. 4c. By further increasing the density (to unrealistic values), the curve approaches that of the absolutely rigid bottom, presented in Fig. 3a. Though the shapes of the backscattering curves are also affected by density variations, the more important influence is that on the magnitude of scattering strength, which increases with increasing density of the sea-floor.

Bottom loss may be considered by introducing a complex sediment sound velocity

$$c_b = c_{bR} + ic_{bI}. \tag{3.11}$$

Figure 4d displays the influence of bottom loss on the theoretical backscattering strength. Bottom losses are chosen for significantly modifiying the curves. Realistic values are represented by the dotted curve while the dashed one is only of theoretical interest. Thus, it may be stated that bottom loss can be ignored in calculating backscattering strengths. Only around the critical angle does smoothing of the dependence on grazing angle occur.

Figures 5a–b show fits of theoretical curves to measured data. The data of Ellis and Crowe (1991) in Fig. 5a are from experiments with explosives in a deep-water area. These data have been chosen because they show the nonmonotonic behaviour of scattering strength as a function of grazing angle, predicted by theory. The measured data can be well fitted by theoretical backscattering strengths deduced from a sea-floor with the standard values of sea-floor velocity and density (solid line) but a somewhat smaller spectral amplitude as (3.10). For large grazing angles, an even better fit can be obtained by assuming a k^{-4} decay of the roughness spectrum, which implies a decrease of backscattering strength with frequency, as discussed above. It should be mentioned that for large grazing angles facet reflection may contribute to the scattering strength, which is not considered by the theory presented.

Mean backscattering strengths in the frequency range 10–100 kHz as a function of grazing angle are given by Bunchuk and Zhitkovskii (1980) for different sea-floors. For our purpose, we use the data referring to a sandy sea-floor, which are represented as a continuous curve for grazing angles between 5° and 75°. In Fig. 5b these data are displayed by crosses in steps of 5°. Both theoretical curves are derived from a roughness spectrum with k^{-3} decay. Again, a better fit at the higher grazing angles 65–75° can be obtained by using a steeper roughness spectrum. However, this does not seem to be reasonable because contributions from specular facet reflection have to be taken into account. Backscattering in the frequency range considered is due to roughness wavelengths of several centimetres, which may be superimposed on longer-scale roughnesses responsible for the above-mentioned facet contribution at larger grazing angles.

The solid curve in Fig. 5b refers to our standard sea-floor parameters, but with a greater roughness spectrum amplitude. The dashed curve represents averaging over sea-floor parameters as in Fig. 3b (solid curve) and is more appropriate to the data representing a mean over different experimental sites. The agreement with the data is better mainly because the peak at the critical angle is smoothed out and the dependence of scattering strength on grazing angle becomes nearly monotonic.

4

Conclusions

A simple scattering theory (perturbation approach), well known in applications such as radar and acoustic scatter from the sea surface, describes surprisingly well important features of acoustic backscatter from a rough sea-floor. Because of the use of over-simplified boundary conditions this has not yet been recognized.

Theoretically derived scattering strengths are strongly dependent on sea-floor parameters, ratios of density and sound velocity of sediment and water, and on the two-dimensional roughness spectrum. However, minimal knowledge about the structure of the sea-floor exists. This is mainly due to the fact that measurements are complicated and cover limited areas only. For the comparison of theory with measured data it has only been possible to show that the necessary assumptions on the sea-floor are reasonable.

For very small grazing angles, the grazing-angle dependent perturbation parameter remains small even for roughness amplitudes of the order of the acoustic wavelength. For this reason and also because of the absence of facet reflections, perturbation theory should be most reliable at small grazing angles. On the other hand, reverberation from long distances is due to backscattering at low grazing angles. For the purpose of predicting reverberation by means of numerical modelling, knowledge of the dependence of the backscattering coefficient, especially on small grazing angles, is of great importance. The perturbation theory predicts the backscattering strength to be independent of the k-dependence of the roughness spectrum at these angles, but dependent on the sound velocity within the sediment.

The presented perturbation theory yields scattering coefficients also for forward scattering. The experimental finding of maximum scattered energy around the angle of specular reflection is in agreement with theory. The longest wavelengths of the roughness field, which in general contain most of the variance, are responsible for nearly specular scattering.

Finally, it should be mentioned that a better understanding of the scattering process may yield information on sea-floor parameters from reverberation measurements by means of inversion techniques.

References

Brekhovskikh, L. and Lysanov, Y. Fundamentals of Ocean Acoustics, 2nd edn. Berlin, Springer, 1991. [ISBN 35405279642]

Bunchuk, A.V. and Zhitkovskii, Y.Y. Sound scattering by the ocean bottom in shallow-water regions (review). *Soviet Physics Acoustics* **26**, 1980: 363–370.

Ellis, D.D. and Crowe, D.V. Bistatic reverberation calculations using a three-dimensional scattering function. *Journal of the Acoustical Society of America* **89**, 1991: 2207–2214.

Mackenzie, K.V. Bottom reverberation for 530- and 1030-cps sound in deep water. *Journal of the Acoustical Society of America* **33**, 1961: 1498–1504.

Ogilvy, J.A. Theory of Wave Scattering from Random Rough Surfaces. Bristol, Hilger, 1991. [ISBN 0750300639]

Robison, A.E. Bottom reverberation in the North Atlantic. DREA TM-75/B. Dartmouth, N.S., Defence Research Establishment Atlantic, 1975. [AD A 022 128]

Thorsos, E.I. Acoustic scattering from a 'Pierson-Moskowitz' sea surface. *Journal of the Acoustical Society of America* **88**, 1990: 335–349.

Urick, R.J. Principles of Underwater Sound, 3rd edn. New York, NY, McGraw-Hill, 1983. [ISBN 0-07-066087-5]

Wright, J.W. A new model for sea clutter. *IEEE Transactions on Antennas and Propagation* **16**, 1968: 217–223.

Appendix A

Model of surface roughness

The purpose of this appendix is to show that the assumptions on the scattering roughness spectrum are reasonable. Assuming that the spectrum extends from a minimum wavenumber to infinity, the variance of bottom roughness becomes (cf. (3.7))

$$\langle \zeta^2 \rangle = G_0 \int_{k_m}^{\infty} k^{-3}\, \mathrm{d}k = \tfrac{1}{2} k_m^{-2} G_0. \tag{A.1}$$

k_m has to be chosen in accordance with acoustic frequencies involved. For the special case of backscattering from k_m at a grazing angle of 45°, the vertical acoustic wavenumber is equal to half of the minimum bottom-roughness wavenumber, and the perturbation parameter turns out to be small,

$$\tfrac{1}{2} k_m \sqrt{\langle \zeta^2 \rangle} = 0.035. \tag{A.2}$$

For acoustic frequencies exceeding the corresponding minimum by more than a factor of 10 the assumption of the perturbation approach begins to fail.

The autocovariance function is the cosine transform of the wavenumber spectrum,

$$\gamma(\xi) = G_0 \int_{k_m}^{\infty} k^{-3} \cos(k\xi)\, \mathrm{d}k. \tag{A.3}$$

Figure 6a displays the theoretical wavenumber spectrum and the corresponding autocorrelation function (normalised autocovariance function). The scales are arbitrary. The minimum wavenumber $k_m = 0.63\ \mathrm{m}^{-1}$ corresponds to a wavelength of 10 m. The autocorrelation function shows an oscillating behaviour, and statistical dependence occurs for wavenumbers exceeding the first zero-crossing at a lag of about 1.6 m.

In order to visualize the bottom structures involved, synthetic representations of a random sea-floor are derived, with the properties stated above. Assuming an isotropic spectral distribution, roughness is only investigated as a function of distance. Synthetic series of bottom roughness are obtained from normally distributed white noise filtered in accordance with the assumed wavenumber dependence and normalized to the total variance. Filtering is performed in the wavenumber space. The length of the series are chosen by 10 m, i.e. the spectral resolution is k_m, the number of data points is 256, extending the spectral range to $128 k_m$ in accordance with the theoretical spectrum of Fig. 6a.

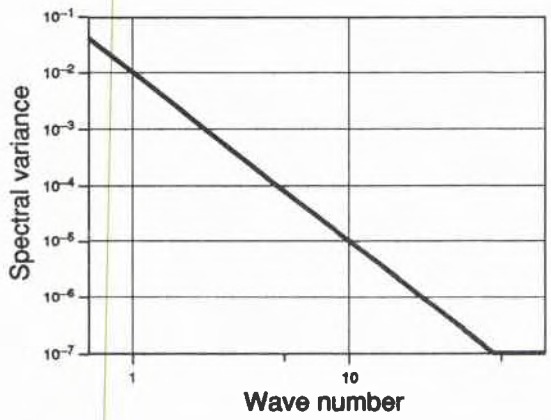

Figure 6a *Variance spectrum and autocorrelation (theoretical). Upper panel: variance spectrum* $G(k) = 0.01k^{-3}$. *Lower panel: respective autocorrelation function.*

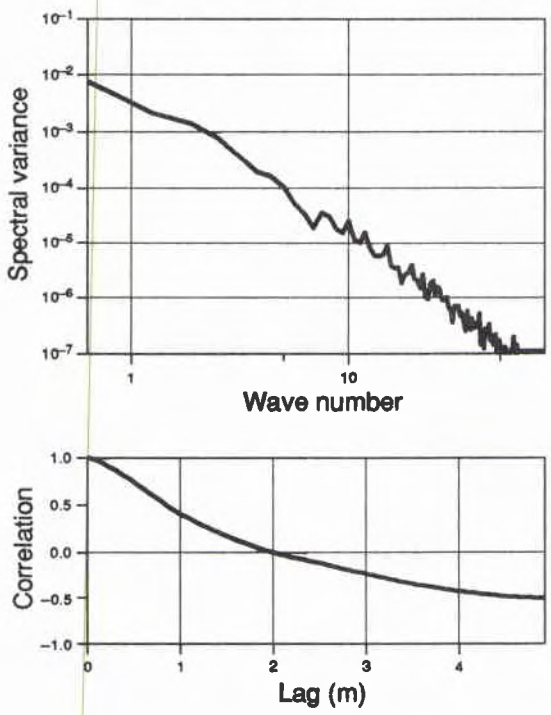

Figure 6b *Variance spectrum and autocorrelation (from simulated data). Upper panel: estimated mean variance spectrum. Lower panel: estimated mean autocorrelation function.*

Fig. 6b displays a mean roughness spectrum and a mean autocorrelation function, as derived by averaging over 10 synthetic representations of the sea-floor. The roughness spectrum is derived from the Fourier coefficients of the space series and the autocorrelation from an estimator, periodically continuing the finite series, in order to allow comparison with the theoretical autocorrelation function of Fig. 6a.

The linear procedures of transforming white noise into frequency space, multiplying by a filter function and backtransforming represents a kind of infinite moving average process. The whole set of random data influences each point of the resultant roughness series. This explains statistical dependences, as shown by the autocorrelation function. Differences between Fig. 6a and Fig. 6b, both in the spectra and in the autocorrelation functions, are due to the finite length of the synthetic series. For the spectra, a flattening occurs at low wavenumbers.

Ensemble averaging, as introduced by perturbation theory, is in practice, replaced by spatial averaging, assuming different parts of the illuminated area yielding statistically independent contributions to scattering strength. Thus, the illumination should extend over areas with large diameters compared to the correlation length of bottom roughness. To be cautious, the correlation length in our model is assumed to be about the length of the space series, which is determined by the minimum wavenumber k_m. To allow the averaging mentioned above the illuminated area has to extend over a number of subareas, each of which may be described by a model as discussed above.

Refering to grazing angles below 40°, acoustic frequencies in the range 75–100 Hz are backscattered from the roughness wavelength of 10 m, corresponding to the minimum wavenumber k_m. With the spectrum (A.1), the perturbation parameter remains small up to a frequency of about 1000 Hz. In order to obtain sufficient statistically independent scattering, the diameter of the illuminated area should be of the order of 100 m. The presented results may be applied to other length and frequency scales by introducing a normalization factor. For example, by reading 'cm' instead of 'm' in Figs. 6a–b, the corresponding frequencies have to be increased by a factor of 100.

Figure 7 displays three representations of bottom roughness, derived from different sets of white-noise data. Over the total range of 10 m, amplitudes of bottom roughness are of the order of 0.2 m. Occasionally, steep slopes occur, which are not unlikely in a rough sea-floor.

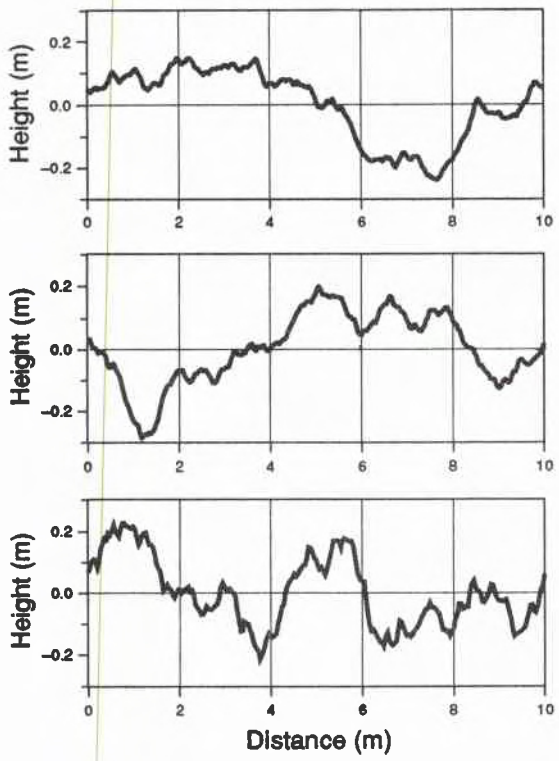

Figure 7 *Synthetic representations of sea-floor roughness, corresponding to the roughness spectrum of Fig. 6b.*

Report no. changed (Mar 2006): SR-194-UU

Initial Distribution for SR-194

Ministries of Defence	
JSPHQ Belgium	2
DND Canada	10
CHOD Denmark	8
MOD France	8
MOD Germany	15
MOD Greece	11
MOD Italy	10
MOD Netherlands	12
CHOD Norway	10
MOD Portugal	5
MOD Spain	2
MOD Turkey	5
MOD UK	20
SECDEF US	60
NATO Authorities	
NAMILCOM	2
SACLANT	3
CINCIBERLANT	1
COMSUBACLANT	1
COMNAVSOUTH	1
SCNR for SACLANTCEN	
SCNR Belgium	1
SCNR Canada	1
SCNR Denmark	1
SCNR Germany	1
SCNR Greece	1
SCNR Italy	1
SCNR Netherlands	1
SCNR Norway	1
SCNR Portugal	1
SCNR Spain	1
SCNR Turkey	1
SCNR UK	1
SCNR US	2
French Delegate	1
SECGEN Rep. SCNR	1
NAMILCOM Rep. SCNR	1
National Liaison Officers	
NLO Canada	1
NLO Denmark	1
NLO Germany	1
NLO Italy	1
NLO Netherlands	1
NLO UK	1
NLO US	1
NLR to SACLANT	
NLR Belgium	1
NLR Canada	1
NLR Denmark	1
NLR Germany	1
NLR Greece	1
NLR Italy	1
NLR Netherlands	1
NLR Norway	1
NLR Portugal	1
NLR Turkey	1
NLR UK	1
Total external distribution	221
SACLANTCEN Library	10
Stock	29
Total number of copies	260